(3)–C(33) [101.6 (3) and 96.7 (3)°].

Acknowledgment. This work was supported by the National Science Foundation (Grant No. CHE77-04981, to M.R.C., and No. CHE75-14460, to J.R.S).

Registry No. $(\mu\text{-H})Os_3(CO)_{10}(\mu\text{-NHSO}_2C_6H_4Me)$, 73017-56-8; $(\mu\text{-H})_2Os_3(CO)_{10}$, 41766-80-7; $MeC_6H_4SO_2N_3$, 941-55-9.

Supplementary Material Available: A table of data-processing formulas and a listing of observed and calculated structure factor amplitudes (21 pages). Ordering information is given on any current masthead page.

Contribution from the Departments of Chemistry, State University of New York at Buffalo, Buffalo, New York 14214, and University of Illinois, Urbana, Illinois 61801

Synthesis, Crystal Structure, and Dynamic Behavior of Tetra-μ-hydrido-μ-[1,2-bis(diphenylphosphino)ethane]-decacarbonyltetraruthenium, an Isomer of $(\mu\text{-H})_4Ru_4(CO)_{10}$(diphos) with a *Bridging* diphos Ligand[1,2]

MELVYN ROWEN CHURCHILL,*[3a] ROMANA A. LASHEWYCZ,[3a] JOHN R. SHAPLEY,*[3b,c] and STEVEN I. RICHTER[3b]

Received November 2, 1979

In the presence of trimethylamine oxide the substitution of $(\mu\text{-H})_4Ru_4(CO)_{12}$ by 1,2-bis(diphenylphosphino)ethane (diphos) occurs rapidly at room temperature and leads to $(\mu\text{-H})_4Ru_4(CO)_{10}(\mu\text{-diphos})$ as the major product. Upon being heated, this compound (isomer II) rearranges to the previously characterized compound $(\mu\text{-H})_4Ru_4(CO)_{10}$(diphos) (isomer I). Isomer II crystallizes in the centrosymmetric monoclinic space group $P2_1/c$ with a = 16.845 (3) Å, b = 14.644 (2) Å, c = 17.469 (3) Å, β = 116.48 (1)°, ρ(obsd) = 1.865 (10) g cm^{-3} and ρ(calcd) = 1.872 g cm^{-3} for V = 3857 Å^3, mol wt 1086.85, and Z = 4. Diffraction data were collected with Mo Kα radiation on a Syntex $P2_1$ diffractometer, and the structure was solved by conventional methods, using the Syntex XTL system. The final discrepancy indices were R_F = 5.9% and R_{wF} = 4.6% for those 2446 reflections with $|F_o| > \sigma(F_o)$. All atoms, including the four bridging hydrides, were located directly. Positional parameters of the hydride ligands were refined, the resulting Ru–(μ-H) bond lengths averaging 1.70 ± 0.12 Å and the Ru–(μ-H)–Ru bond angles averaging 124 ± 9°. The hydrido-bridged ruthenium–ruthenium vectors range from 2.923 (2) to 3.048 (2) Å, while the nonhydrido-bridged Ru–Ru bonds are 2.779 (2) and 2.782 (2) Å. The diphos ligand takes up a bridging position between Ru(1) and Ru(2), the two ruthenium–phosphorus bond lengths being 2.356 (4) and 2.335 (5) Å. The $(\mu\text{-H})_4Ru_4$ core of the molecule takes up the asymmetric (idealized C_s symmetry) form, as found in $(\mu\text{-H})_4Ru_4(CO)_{10}$(diphos) (isomer I), rather than the symmetric (D_{2d}) configuration found in other $H_4Ru_4L_{12}$ species. The hydride ligands in $(\mu\text{-H})_4Ru_4(CO)_{10}(\mu\text{-diphos})$ are fluxional. Complete equilibration is evident at room temperature (τ 27.3, triplet, J = 3 Hz). Various stages of the equilibration are observable at lower temperatures, but a static spectrum was not achieved even at −131 °C. Spectral changes below −70 °C can be interpreted in terms of edge-to-edge movement of one hydride ligand (ΔG^* = 7.2 kcal/mol) together with conformational changes in the backbone of the diphos ligand (ΔG^* = 9.1 kcal/mol).

Introduction

We have previously reported the crystal structure and dynamic ^{1}H NMR spectra of $(\mu\text{-H})_4Ru_4(CO)_{10}$(diphos).[2,4] The X-ray study showed that the diphos ligand chelates to one ruthenium atom (see I) and that the $(\mu\text{-H})_4Ru_4$ core of the molecule adopts configuration III (idealized C_s symmetry) rather than the more symmetrical configuration IV (idealized D_{2d} symmetry) inferred for $(\mu\text{-H})_4Ru_4(CO)_{12}$, $(\mu\text{-H})_4Ru_4(CO)_{11}[P(OMe)_3]$, and $(\mu\text{-H})_4Ru_4(CO)_{10}(PPh_3)_2$.[5] The NMR spectra showed that the hydride ligands scramble over the metal framework, and the spectral changes were interpreted in terms of an edge–terminal–edge scrambling mechanism. The previous compound (I) was prepared from the direct reaction of $(\mu\text{-H})_4Ru_4(CO)_{12}$ and diphos at 60 °C. Subsequently, we have found that in the presence of trimethylamine *N*-oxide substitution occurs at 25 °C[6] but that it leads to an isomeric product shown herein to be $(\mu\text{-H})_4Ru_4(CO)_{10}(\mu\text{-diphos})$ (see II). In addition we now report

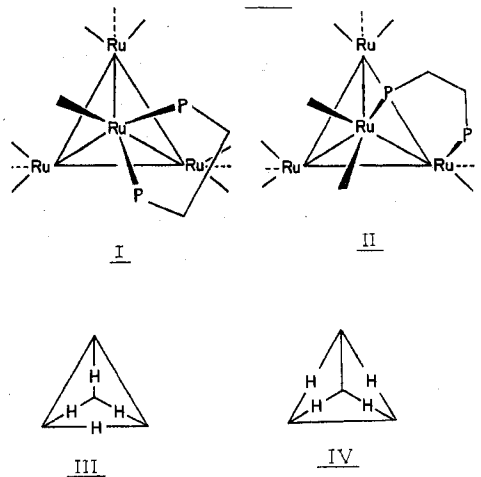

(1) This article constitutes part 4 of our series "Crystallographic Studies on Ruthenium Carbonyl Hydrides". For the previous contribution, see ref 2.
(2) Part 3: Churchill, M. R.; Lashewycz, R. A. *Inorg. Chem.* **1978**, *17*, 1950.
(3) (a) SUNY at Buffalo. (b) University of Illinois. (c) A. P. Sloan Foundation Fellow, 1978–1980; Camille and Henry Dreyfus Teacher-Scholar, 1978–1983.
(4) Shapley, J. R.; Richter, S. I.; Churchill, M. R.; Lashewycz, R. A. *J. Am. Chem. Soc.* **1977**, *99*, 7384.
(5) (a) Wilson, R. D.; Wu, S. M.; Love, R. A.; Bau, R. *Inorg. Chem.* **1978**, *17*, 1271. (b) Knox, S. A. R.; Kaesz, H. D. *J. Am. Chem. Soc.* **1971**, *93*, 4594.
(6) The ability of trimethylamine *N*-oxide to promote carbonyl substitution reactions under mild conditions is well documented. See: (a) Shvo, Y.; Hazum, E. *J. Chem. Soc., Chem. Commun.* **1975**, 829. (b) Koell, V. *J. Organomet. Chem.* **1977**, *133*, 53. (c) Stuntz, G. F.; Shapley, J. R.; Pierpont, C. G. *Inorg. Chem.* **1978**, *17*, 2596. (d) Johnson, B. F. G.; Lewis, J.; Pippard, D. *J. Organomet. Chem.* **1978**, *160*, 263. (e) Blumer, D. J.; Barnett, K. W.; Brown, T. L. *J. Organomet. Chem.* **1978**, *173*, 71.

0020-1669/80/1319-1277$01.00/0

that $(\mu\text{-H})_4Ru_4(CO)_{10}(\mu\text{-diphos})$ (isomer II) also displays core configuration III as well as highly mobile hydride ligands. It is relevant to note, at this point, that two isomers (of C_2 and C_{3v} symmetry) have been reported for the $(\mu\text{-H})_3Ru_4(CO)_{12}^-$ anion.[7]

Experimental Section

A. Synthetic Procedures. The compound $(\mu\text{-H})_4Ru_4(CO)_{12}$ was prepared by the method of Kaesz and co-workers.[8] The compounds $Me_3NO{\cdot}2H_2O$ (Aldrich), $Ph_2PCH_2CH_2PPh_2$ (Strem), and PPh_2Me (Strem) were used as received. Elemental analyses were carried out at the University of Illinois by Mr. J. Nemeth. IR spectra were obtained on solutions in 0.5-mm path length NaCl cavity cells with a Perkin-Elmer 467 spectrophotometer. NMR spectra were recorded with Varian HA-100 (^1H) and XL-100 (^{31}P) spectrometers. Field-desorption mass spectra were obtained with a Varian 731 spectrometer by Mr. J. Carter Cook, Jr.

$(\mu\text{-H})_4Ru_4(CO)_{10}(\mu\text{-diphos})$. $(\mu\text{-H})_4Ru_4(CO)_{12}$ (60 mg, 0.09 mmol) and $Ph_2PCH_2CH_2PPh_2$ (40 mg, 0.1 mmol) were dissolved in dichloromethane (200 mL) at room temperature. This solution was stirred while a solution of $Me_3NO{\cdot}2H_2O$ (18 mg, 0.16 mmol) in acetonitrile (75 mL) was added in 2-mL portions over a period of 20 min. The initially clear yellow solution turned orange during the addition, after which it was evaporated to dryness. The residue was dissolved in a small amount of dichloromethane and added to a silica gel column (2 × 10 cm) prepared with carbon tetrachloride. Elution was continued with carbon tetrachloride to remove the yellow band of unreacted $(\mu\text{-H})_4Ru_4(CO)_{12}$. Elution with benzene developed a red band, which was collected, and the solution was evaporated. Recrystallization of the residue from dichloromethane/methanol yielded red crystals of $(\mu\text{-H})_4Ru_4(CO)_{10}(\mu\text{-diphos})$ (30 mg, 34%). Other products were more polar and were not characterized. The field-desorption mass spectrum exhibited a molecular ion pattern at m/e 1083 ± 5 (calcd (^{101}Ru) m/e 1086). IR (chloroform): ν_{CO} 2070 (s), 2051 (s), 2029 (vs), 2007 (s), 1988 (m, br), 1970 (m), 1966 (m), 1943 (sh) cm^{-1}. ^1H NMR (dichloromethane) (μ-H): τ 27.3 (t, J = 3 Hz) at 28 °C. Anal. Calcd for $C_{36}H_{28}O_{10}P_2Ru_4$: C, 39.78; H, 2.60; P, 5.70. Found: C, 40.00; H, 2.62; P, 6.00.

In solution over a period of days at room temperature or in 2–3 h at ~60 °C there is clean isomerization to isomer I, $(\mu\text{-H})_4Ru_4(CO)_{10}(diphos)$.[2,4] Spectral data for the latter under ambient conditions are as follows: IR ν_{CO} 2075 (s), 2046 (vs), 2023 (vs), 2005 (s), 1986 (m, br), 1945 (w) cm^{-1}; ^1H NMR (μ-H) τ 25.8 (3 H, br), 29.2 (1 H, t, J = 9 Hz). ^{31}P NMR data for both isomers are shown in Table VII.

$(\mu\text{-H})_4Ru_4(CO)_{10}(PPh_2Me)_2$. A cyclohexane solution (200 mL) of $(\mu\text{-H})_4Ru_4(CO)_{12}$ (200 mg, 0.27 mmol) and PPh_2Me (100 mg, 0.5 mmol) was heated under reflux in a nitrogen atmosphere for 4 h. The solution was cooled and evaporated to dryness. The residue was dissolved in a small amount of dichloromethane and applied to a silica gel column. Successive elution with benzene, dichloromethane, and acetone separated orange-red bands containing the compounds $(\mu\text{-H})_4Ru_4(CO)_{12-x}(PPh_2Me)_x$, x = 1, 2, and 3, respectively. The compounds were identified by their hydride ^1H NMR signals, a doublet, a triplet, and a quartet, respectively, due to P–H coupling.[5b] ^{31}P NMR data for $(\mu\text{-H})_4Ru_4(CO)_{10}(PPh_2Me)_2$ are shown in Table VII.

B. Collection of the X-ray Diffraction Data. The crystal selected for the X-ray structural analysis was a small red needle of approximate dimensions 0.20 × 0.07 × 0.05 mm. It was mounted along its extended axis on a thin glass fiber which was inserted into a brass pin with beeswax and placed in a eucentric goniometer. Preliminary precession and cone-axis photographs provided approximate unit cell parameters and indicated that the crystal belonged to the monoclinic crystal system; i.e., it has $2/m$ (C_{2h}) Laue symmetry. The systematic absences $h0l$ for $l = 2n + 1$ and $0k0$ for $k = 2n + 1$ uniquely indicate the space group $P2_1/c$ (C_{2h}^5; No. 14).

The crystal was transferred to a Syntex $P2_1$ automated four-circle diffractometer. The crystal was centered optically. Accurate unit cell parameters and the orientation matrix were determined as described by Churchill, Lashewycz, and Rotella.[9a] Details appear in Table I. Following data collection, several relatively intense and close-to-axial reflections were measured at 10° intervals around their diffraction vector (ψ). The variation in intensity was, in each case, less than 5%. This and the estimate of $\mu\Delta t$ = 0.032 (i.e., 16.31 × 0.002) about the rotation axis (ϕ) indicate that absorption corrections may safely be neglected.

Table I. Data for the X-ray Diffraction Study of $(\mu_2\text{-H})_4Ru_4(CO)_{10}(\mu_2\text{-diphos})$

(A) Crystal Data

cryst system: monoclinic	V = 3857 (1) Å^3
space group: $P2_1/c$ (C_{2h}^5; No. 14)	T = 22 °C
	Z = 4
a = 16.845 (3) Å	mol wt 1086.85
b = 14.644 (2) Å	ρ(obsd)[a] = 1.865 (10) g cm^{-3}
c = 17.469 (3) Å	ρ(calcd) = 1.872 g cm^{-3}
β = 116.48 (1)°	

(B) Intensity Data

radiation: Mo Kα ($\bar{\lambda}$ = 0.710 73 Å)
monochromator: highly-oriented graphite
rflctns measd: $\pm h, +k, +l$
max 2θ: 35°
min 2θ: 3.5°
scan type: coupled θ(crystal)–2θ(counter)
scan speed: 2.0°/min
scan range: symmetrical, $[2.0 + \Delta(\alpha_2 - \alpha_1)]$°
rflctns collected: 3213 total, 2824 independent
abs coeff: 16.31 cm^{-1}; no absorption correction made (see text)

[a] Measured by flotation in aqueous barium iodide.

Systematically absent reflections were examined and rejected (all were within 3σ of zero intensity) as were the check reflections. Laue-equivalent reflections were averaged [$R(I)$ = 2.3% for 123 pairs of reflections], and all data were reduced to their net intensities (I) and their estimated standard deviations ($\sigma(I)$) as shown in eq 1 and 2, where CT is the count associated with the θ–2θ scan, B_1 and B_2

$$I = \mathrm{CT} - \tau(B_1 + B_2) \tag{1}$$

$$\sigma(I) = [\mathrm{CT} + \tau^2(B_1 + B_2)]^{1/2} \tag{2}$$

are the initial and final background counts, and τ is the ratio of time taken for the θ–2θ scan to the total time for which the backgrounds of the reflection were measured (=2.0 in the present study). All data were corrected for Lorentz and polarization factors, the form of the Lp factor being that given in eq 3 and applied to I as shown in eq 4. Equation 3 assumes that the equatorially mounted monochromator

$$Lp = \frac{0.5}{\sin 2\theta}\left[\left(\frac{1 + \cos^2 2\theta_M \cos^2 2\theta}{1 + \cos^2 2\theta_M}\right) + \left(\frac{1 + |\cos 2\theta_M| \cos^2 2\theta}{1 + |\cos 2\theta_M|}\right)\right] \tag{3}$$

$$|F_o| = (I/Lp)^{1/2} \tag{4}$$

(for which $2\theta_M$ = 12.2° for Mo Kα radiation) is 50% mosaic and 50% perfect in the reflecting direction. Any reflection with $0 > I > -400$ counts had its intensity reset to zero. Three reflections with $I < -400$ counts were assumed to be systematically in error and were deleted.

C. Solution and Refinement of the Structure. All calculations were performed by using the Syntex XTL structure determination sytem comprised of the following components: (a) an in-house Data General NOVA 1200 computer with 24 K of 16-bit words and with a parallel floating-point processor for 32- or 64-bit arithmetic, (b) a Diablo moving-head disk unit with 1.2 million 16-bit words, (c) a Versatec electrostatic printer/plotter, and (d) the XTL interactive crystallographic program package[9b] as modified by our research group at Buffalo. The analytical scattering factors of Cromer and Waber[10a]

(7) Jackson, P. F. J.; Johnson, B. F. G.; Lewis, J.; McPartlin, M.; Nelson, W. J. H. *J. Chem. Soc., Chem. Commun.* **1978**, 920–1.
(8) Koepke, J. W.; Johnson, J. R.; Knox, S. A. R.; Kaesz, H. D. *J. Am. Chem. Soc.* **1975**, *97*, 3947.
(9) (a) Churchill, M. R.; Lashewycz, R. A.; Rotella, F. J. *Inorg. Chem.* **1977**, *16*, 265. (b) "Syntex XTL Operations Manual", 2nd ed.; Syntex Analytical Instruments: Cupertino, CA, 1976.

Table II. Final Positional Parameters (with Esd's)[a] for $(\mu_2\text{-H})_4Ru_4(CO)_{10}(\mu_2\text{-diphos})$

atom	x	y	z	atom	x	y	z
Ru(1)	0.183 92 (8)	0.174 98 (9)	−0.223 27 (8)	C(109)	0.2781 (11)	0.5513 (12)	−0.2278 (11)
Ru(2)	0.353 46 (8)	0.072 93 (9)	−0.191 78 (8)	C(110)	0.2240 (10)	0.5780 (12)	−0.1928 (10)
Ru(3)	0.182 11 (8)	−0.001 53 (10)	−0.312 61 (8)	C(111)	0.1594 (11)	0.5204 (12)	−0.1954 (10)
Ru(4)	0.237 35 (8)	−0.005 18 (10)	−0.136 94 (8)	C(112)	0.1498 (10)	0.4354 (11)	−0.2334 (9)
C(11)	0.0622 (12)	0.1915 (11)	−0.2520 (10)	C(201)	0.5385 (9)	0.1984 (10)	−0.1735 (9)
O(11)	−0.0104 (9)	0.2031 (9)	−0.2696 (9)	C(202)	0.5631 (10)	0.2814 (11)	−0.1295 (10)
C(12)	0.2198 (11)	0.2456 (13)	−0.1246 (12)	C(203)	0.6510 (11)	0.2976 (12)	−0.0705 (11)
O(12)	0.2384 (10)	0.2860 (10)	−0.0627 (8)	C(204)	0.7142 (10)	0.2319 (12)	−0.0515 (10)
C(21)	0.4300 (12)	0.0967 (13)	−0.0780 (12)	C(205)	0.6930 (11)	0.1517 (12)	−0.0916 (10)
O(21)	0.4782 (9)	0.1124 (9)	−0.0080 (9)	C(206)	0.6039 (10)	0.1325 (10)	−0.1514 (9)
C(22)	0.4215 (11)	−0.0281 (13)	−0.1924 (10)	C(207)	0.4368 (10)	0.1382 (11)	−0.3428 (10)
O(22)	0.4638 (8)	−0.0869 (9)	−0.1937 (8)	C(208)	0.4905 (10)	0.1889 (11)	−0.3689 (10)
C(31)	0.0746 (13)	−0.0473 (12)	−0.3197 (11)	C(209)	0.4933 (11)	0.1664 (13)	−0.4465 (11)
O(31)	0.0079 (8)	−0.0752 (11)	−0.3256 (8)	C(210)	0.4443 (11)	0.1007 (12)	−0.4969 (11)
C(32)	0.1503 (10)	0.0062 (13)	−0.4314 (12)	C(211)	0.3905 (11)	0.0472 (12)	−0.4719 (11)
O(32)	0.1305 (10)	0.0035 (14)	−0.5020 (9)	C(212)	0.3879 (11)	0.0668 (13)	−0.3954 (11)
C(33)	0.2288 (11)	−0.1214 (14)	−0.2966 (11)	H(1)[b]	0.2688	0.2141	−0.3724
O(33)	0.2514 (9)	−0.1934 (10)	−0.2921 (8)	H(2)	0.2667	0.3174	−0.3929
C(41)	0.1397 (12)	−0.0623 (12)	−0.1268 (10)	H(3)	0.3708	0.3112	−0.2257
O(41)	0.0875 (8)	−0.1012 (9)	−0.1177 (8)	H(4)	0.4068	0.3233	−0.2929
C(42)	0.2954 (11)	0.0363 (11)	−0.0254 (12)	H(102)	0.1285	0.4332	−0.4425
O(42)	0.3306 (9)	0.0635 (9)	0.0449 (9)	H(103)	0.0082	0.4450	−0.5806
C(43)	0.3047 (13)	−0.1122 (15)	−0.1173 (11)	H(104)	−0.0986	0.3334	−0.6370
O(43)	0.3424 (8)	−0.1794 (10)	−0.1038 (8)	H(105)	−0.0868	0.1999	−0.5574
H(12)	0.292 (7)	0.159 (7)	−0.191 (6)	H(106)	0.0313	0.1828	−0.4201
H(13)	0.148 (7)	0.116 (7)	−0.308 (7)	H(108)	0.3061	0.4521	−0.2964
H(14)	0.159 (7)	0.085 (7)	−0.166 (6)	H(109)	0.3281	0.5913	−0.2223
H(23)	0.265 (7)	0.055 (7)	−0.293 (6)	H(110)	0.2321	0.6387	−0.1666
P(1)	0.1885 (3)	0.2919 (3)	−0.3139 (3)	H(111)	0.1192	0.5391	−0.1713
P(2)	0.4257 (3)	0.1697 (3)	−0.2467 (3)	H(112)	0.1049	0.3934	−0.2339
C(1)	0.2754 (10)	0.2751 (10)	−0.3472 (9)	H(202)	0.5174	0.3279	−0.1417
C(2)	0.3729 (10)	0.2824 (10)	−0.2744 (10)	H(203)	0.6669	0.3575	−0.0411
C(101)	0.0928 (10)	0.3038 (11)	−0.4172 (9)	H(204)	0.7756	0.2433	−0.0096
C(102)	0.0842 (11)	0.3835 (12)	−0.4654 (11)	H(205)	0.7380	0.1050	−0.0809
C(103)	0.0137 (13)	0.3912 (14)	−0.5462 (12)	H(206)	0.5882	0.0714	−0.1767
C(104)	−0.0490 (12)	0.3256 (14)	−0.5803 (12)	H(208)	0.5249	0.2400	−0.3339
C(105)	−0.0424 (12)	0.2487 (14)	−0.5331 (12)	H(209)	0.5318	0.2018	−0.4638
C(106)	0.0291 (11)	0.2380 (12)	−0.4520 (10)	H(210)	0.4466	0.0885	−0.5514
C(107)	0.2065 (10)	0.4074 (11)	−0.2679 (9)	H(211)	0.3535	−0.0023	−0.5088
C(108)	0.2687 (11)	0.4677 (12)	−0.2678 (10)	H(212)	0.3508	0.0298	−0.3763

[a] Esd's, shown in parentheses, are right adjusted to the least significant digit of the preceding number. They are derived from the inverse of the final least-squares matrix. [b] The hydrogen atoms of the diphos ligand were included in the final model in their idealized calculated positions.

for neutral ruthenium, oxygen, carbon, and hydrogen were used throughout the analysis; both the real ($\Delta f'$) and imaginary ($\Delta f''$) components of anomalous dispersion[10b] were included for all nonhydrogen atoms. The function minimized during least-squares refinement was $\sum w(|F_o| - |F_c|)^2$, where the weights (w) are defined by eq 5, and $\sigma_c(F_o)$ is based solely upon counting statistics. The "ignorance factor" (p) was set at a value of 0.0175.

$$w = [[\sigma_c(F_o)]^2 + (p|F_o|)^2]^{-1} \quad (5)$$

Discrepancy indices used below are defined in eq 6 and 7. The "goodness-of-fit" (GOF) is defined in eq 8; here, NO is the number of observations and NV is the number of variables.

$$R_F = \left[\frac{\sum||F_o| - |F_c||}{\sum w|F_o|}\right] \times 100\ (\%) \quad (6)$$

$$R_{wF} = \left[\frac{\sum w(|F_o| - |F_c|)^2}{\sum w|F_o|^2}\right]^{1/2} \times 100\ (\%) \quad (7)$$

$$\text{GOF} = \left[\frac{\sum w(|F_o| - |F_c|)^2}{\text{NO} - \text{NV}}\right]^{1/2} \quad (8)$$

The positions of the four ruthenium atoms were determined from an unsharpened three-dimensional Patterson synthesis. Full-matrix least-squares refinement of the scale factor along with positional and anisotropic thermal parameters of the ruthenium atoms led to R_F = 28.7%. A difference Fourier synthesis revealed the positions of all remaining nonhydrogen atoms. Continued refinement, including positional and isotropic thermal parameters of the newly found atoms, resulted in R_F = 9.8%. The use of anisotropic thermal parameters for all nonhydrogen atoms other than carbon atoms of the phenyl rings led to convergence with R_F = 6.4%. A difference Fourier synthesis now led to the unambiguous location of all hydrogen atoms in the structure. Hydrogen atoms of the diphos ligand were included in our model in their idealized positions (i.e., with a regular sp^2 or sp^3 geometry and with d(C–H) = 0.95 Å).[11] Their isotropic thermal parameters were set at a value 1.0 Å^2 larger than that of the carbon atom to which they were attached. The four hydride ligands were included in their observed positions; their isotropic thermal parameters were set at 2.0 Å^2, but their positional parameters were included in the refinement. Continued refinement led to final convergence with R_F = 5.9%, R_{wF} = 4.6%, and GOF = 1.28 for those 2446 reflections with $|F_o| > \sigma(F_o)$.

For confirmation of the accurate refined positions of the four hydride ligands, they were removed from the model; refinement to convergence led to statistically significant[10c] increased residuals: R_F = 6.4%, R_{wF} = 4.8%, and GOF = 1.33. Finally, with the hydride ligands still omitted, a difference Fourier synthesis was performed on the basis of those 790 data with $(\sin\theta)/\lambda < 0.30$ Å^{-1}. Peaks of height 0.41,

(10) "International Tables for X-Ray Crystallography"; Kynoch Press: Birmingham, England, 1974; Vol. IV: (a) pp 99–101; (b) pp 149–50; (c) pp 288–92.

(11) Churchill, M. R. *Inorg. Chem.* **1973**, *12*, 1213.

Table III. Thermal Parameters[a-c] ($Å^2$) for $(\mu_2\text{-H})_4Ru_4(CO)_{10}(\mu_2\text{-diphos})$

atom	B_{11}	B_{22}	B_{33}	B_{12}	B_{13}	B_{23}
Ru(1)	2.68 (7)	2.13 (7)	2.99 (7)	0.12 (6)	1.68 (6)	0.23 (6)
Ru(2)	2.39 (7)	2.03 (7)	2.77 (7)	−0.11 (6)	1.40 (6)	0.10 (6)
Ru(3)	2.62 (7)	2.64 (7)	2.61 (7)	−0.18 (6)	1.32 (5)	−0.10 (6)
Ru(4)	2.99 (7)	2.28 (7)	2.78 (7)	0.04 (6)	1.70 (6)	0.28 (6)
C(11)	3.2 (10)	2.2 (9)	4.5 (10)	−0.6 (8)	1.5 (8)	1.2 (8)
O(11)	2.4 (6)	6.8 (9)	10.0 (10)	0.4 (6)	3.2 (7)	1.0 (7)
C(12)	4.1 (10)	4.3 (11)	2.6 (10)	0.4 (9)	2.0 (9)	1.4 (9)
O(12)	9.2 (10)	6.3 (9)	4.2 (8)	−1.2 (7)	3.1 (8)	−1.0 (7)
C(21)	3.4 (10)	4.5 (11)	3.3 (10)	0.6 (9)	2.2 (9)	1.2 (10)
O(21)	5.8 (9)	6.4 (8)	3.4 (7)	−0.4 (7)	0.9 (6)	0.0 (7)
C(22)	2.6 (9)	4.7 (13)	3.2 (9)	−0.4 (8)	2.4 (8)	−0.3 (8)
O(22)	5.4 (8)	3.9 (8)	7.3 (8)	1.4 (6)	3.9 (7)	−0.2 (6)
C(31)	4.6 (11)	4.4 (11)	4.3 (10)	0.8 (9)	2.5 (9)	0.6 (8)
O(31)	2.8 (7)	10.7 (11)	8.2 (9)	−0.7 (7)	3.0 (7)	0.4 (8)
C(32)	3.5 (9)	5.8 (11)	2.4 (10)	0.2 (9)	1.5 (8)	1.9 (10)
O(32)	9.7 (10)	14.1 (13)	3.0 (7)	1.3 (10)	2.1 (8)	2.3 (10)
C(33)	3.1 (9)	3.6 (11)	3.7 (10)	−0.5 (9)	1.4 (8)	−2.4 (10)
O(33)	7.3 (8)	3.0 (7)	5.4 (8)	1.4 (7)	2.5 (6)	−1.2 (7)
C(41)	4.4 (10)	2.6 (9)	3.6 (9)	−0.6 (8)	2.8 (8)	0.8 (8)
O(41)	5.1 (7)	6.0 (8)	8.1 (9)	−2.3 (6)	4.2 (7)	0.9 (7)
C(42)	4.4 (10)	1.7 (9)	3.8 (11)	−0.5 (7)	2.8 (9)	0.3 (8)
O(42)	6.7 (8)	5.3 (8)	4.5 (8)	−0.3 (7)	2.8 (7)	−0.5 (7)
C(43)	4.8 (11)	5.2 (13)	3.6 (10)	0.4 (10)	2.9 (9)	−1.3 (10)
O(43)	5.1 (8)	4.4 (8)	6.1 (8)	1.8 (6)	3.3 (6)	0.2 (6)
P(1)	2.7 (2)	2.0 (2)	3.0 (2)	0.1 (2)	1.6 (2)	0.0 (2)
P(2)	2.6 (2)	2.3 (2)	3.3 (2)	−0.0 (2)	1.8 (2)	−0.0 (2)
C(1)	3.6 (9)	1.8 (8)	3.7 (9)	0.3 (7)	2.4 (8)	−0.1 (7)
C(2)	2.1 (8)	2.2 (9)	3.7 (9)	−0.0 (7)	1.3 (8)	−0.2 (7)

atom	B	atom	B	atom	B	atom	B
C(101)	2.7 (3)	C(201)	2.1 (3)	C(107)	3.0 (4)	C(207)	3.1 (4)
C(102)	4.4 (4)	C(202)	3.3 (4)	C(108)	4.1 (4)	C(208)	3.3 (4)
C(103)	5.7 (5)	C(203)	4.2 (4)	C(109)	4.6 (4)	C(209)	4.6 (4)
C(104)	5.4 (4)	C(204)	3.7 (4)	C(110)	3.8 (4)	C(210)	4.3 (4)
C(105)	4.9 (4)	C(205)	4.0 (4)	C(111)	4.3 (4)	C(211)	4.7 (4)
C(106)	3.8 (4)	C(206)	2.8 (4)	C(112)	3.3 (4)	C(212)	4.3 (4)
H(12)	2.0	H(1)	4.0	H(14)	2.0	H(3)	4.2
H(13)	2.0	H(2)	4.0	H(23)	2.0	H(4)	4.2
H(102)	4.9	H(202)	4.1	H(108)	5.1	H(208)	4.1
H(103)	6.4	H(203)	5.1	H(109)	5.4	H(209)	5.2
H(104)	6.0	H(204)	4.9	H(110)	5.1	H(210)	5.4
H(105)	5.6	H(205)	4.8	H(111)	5.2	H(211)	5.4
H(106)	4.6	H(206)	4.0	H(112)	4.3	H(212)	5.2

[a] The anisotropic thermal parameter is defined by the following expression: $\exp[-0.25(B_{11}h^2a^{*2} + B_{22}k^2b^{*2} + B_{33}l^2c^{*2} + 2B_{12}hka^*b^* + 2B_{13}hla^*c^* + 2B_{23}klb^*c^*)]$. [b] Isotropic thermal parameters are given for the phenyl carbon atoms and for all hydrogen atoms. For those hydrogen atoms in the diphos ligand, B was fixed at a value 1.0 $Å^2$ greater than the isotropic factor for the corresponding carbon to which the hydrogen is bound. [c] Esd's, shown in parentheses, are right adjusted to the least significant digit of the preceding number.

0.46, 0.45, and 0.53 e $Å^{-3}$ were found at the refined positions of H(12), H(13), H(14), and H(23), respectively. The appearance of these features is illustrated clearly in Figure 1. *The positions of the hydride ligands are thus determined unambiguously.*

Final positional and thermal parameters are collected in Tables II and III.

Discussion of the Solid-State Molecular Structure of $(\mu\text{-H})_4Ru_4(CO)_{10}(\mu\text{-diphos})$

The crystal is composed of discrete molecular units of $(\mu\text{-H})_4Ru_4(CO)_{10}(\mu\text{-diphos})$ which are mutually separated by normal van der Waals distances; there are no abnormally short interatomic contacts. A stereoscopic view of the entire molecule appears in Figure 2. The essential details of the atomic labeling scheme are given in Figure 3, which shows the molecule projected on to the Ru(2)–Ru(3)–Ru(4) plane. (Phenyl groups of the diphos ligand and the hydrogen atoms associated with C(1) and C(2) have been omitted from this diagram, in the interest of clarity.) Carbon atoms of the phenyl groups are labeled cyclically, the first digit indicating the phosphorus atom with which that carbon atom is associated. Thus C(101) and C(107) are each bonded directly to P(1), the two phenyl groups being defined by atoms C(101) through C(106) and C(107) through C(112). Likewise, C(201) and C(207) are linked directly to P(2), the two associated phenyl rings being defined by C(201) through C(206) and C(207) through C(212). Hydrogen atoms of the diphos ligand are numbered identically with their attached carbon atoms. Interatomic distances and angles are given in Tables IV and V.

The $(\mu\text{-H})_4Ru_4(CO)_{10}(\mu\text{-diphos})$ molecule is topologically equivalent to $(\mu\text{-H})_4Ru_4(CO)_{10}(diphos)^2$ (isomer I) except that the diphos ligand now spans the Ru(1)–Ru(2) vector, rather than acting as a chelating ligand on Ru(1), and there has been a concomitant transfer of a carbonyl ligand from Ru(2) to Ru(1). Three classical two-electron donor ligands (two carbonyl ligands and P(1)) are bonded to Ru(1), two carbonyl ligands and P(2) are bonded to Ru(2), and three terminal carbonyl ligands are bonded to Ru(3) and to Ru(4).

The ruthenium–ruthenium distances fall into two distinct classes. The two nonhydrido-bridged Ru–Ru bonds are "short" with the values Ru(2)–Ru(4) = 2.779 (2) Å and Ru(3)–Ru(4) = 2.782 (2) Å; the average value is 2.781 ± 0.002 Å (cf. 2.791 ± 0.007 Å in I).[2] The four remaining ruthenium–ruthenium vectors (i.e., those bridged by μ_2-hydride ligands) are "long", individual values being Ru(1)–Ru(2) = 3.048 (2) Å, Ru(1)–Ru(3) = 3.012 (2) Å, Ru(1)–Ru(4) = 2.972 (2) Å, and

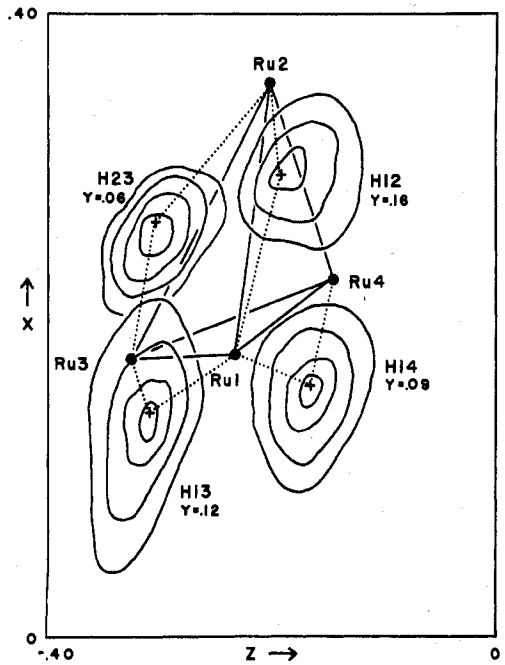

Figure 1. Difference Fourier synthesis, showing the locations of the four bridging hydride ligands. This is based upon the model with hydride ligands (only) omitted, using those 790 data with $(\sin\theta)/\lambda < 0.30$ Å^{-1}. Contours are at 0.1 e Å^{-3} intervals, the lowest such contour being 0.2 e Å^{-3}. (The highest contours for H(13) and H(14) correspond to 0.45 e Å^{-3}, however.) The refined positions of ruthenium atoms and hydride ligands are indicated by filled circles and crosses, respectively.

Ru(2)–Ru(3) = 2.923 (2) Å. The average value of 2.989 ± 0.054 Å is 0.208 Å longer than the average nonbridged distance of 2.781 ± 0.002 Å and may be compared to the average Ru–H–Ru distance of 2.970 ± 0.037 Å found in isomer I.[2]

The four bridging ligands were located directly from the structural analysis, and their positional parameters were refined. All behaved well, and their positional parameters converged. The four Ru–H–Ru systems appear to be symmetrical, the interatomic distances and angles being as follows: Ru(1)–H(12) = 1.66 (12) Å, Ru(2)–H(12) = 1.63 (12) Å, Ru(1)–H(12)–Ru(2) = 135 (7)°; Ru(1)–H(13) = 1.58 (11) Å, Ru(3)–H(13) = 1.84 (11) Å, Ru(1)–H(13)–Ru(3) = 123 (7)°; Ru(1)–H(14) = 1.80 (11) Å, Ru(4)–H(14) = 1.78 (11) Å, Ru(1)–H(14)–Ru(4) = 112 (6)°; Ru(2)–H(23) = 1.76 (11) Å, Ru(3)–H(23) = 1.52 (12) Å, Ru(2)–H(23)–Ru(3) = 126 (7)°. The average Ru–(μ-H) distance is 1.70 ± 0.12 Å, and the average Ru–H–Ru angle is 124 ± 9° (cf. mean values of 1.76 ± 0.06 Å and 115 ± 4° for isomer I).[2]

As has been indicated previously, as a result of our studies of $(\mu\text{-H})_3Os_3W(CO)_{11}(\eta^5\text{-}C_5H_5)$[12] and $(\mu\text{-H})Os_3W(CO)_{12}(\eta^5\text{-}C_5H_5)$,[13] the diagrams III and IV are oversimplifications, insofar as each bridging hydride ligand may take up a number

Table IV. Interatomic Distances and Esd's for $(\mu_2\text{-H})_4Ru_4(CO)_{10}(\mu_2\text{-diphos})$

atom	dist, Å	atom	dist, Å
(a) "Short" Ruthenium–Ruthenium			
Ru(2)–Ru(4)	2.779 (2)	Ru(3)–Ru(4)	2.782 (2)
average = 2.781 ± 0.002 Å			
(b) "Long" Ruthenium–Ruthenium			
Ru(1)–Ru(2)	3.048 (2)	Ru(1)–Ru(4)	2.972 (2)
Ru(1)–Ru(3)	3.012 (2)	Ru(2)–Ru(3)	2.923 (2)
average = 2.989 ± 0.054 Å			
(c) Ruthenium–Hydrogen			
Ru(1)–H(12)	1.66 (12)	Ru(1)–H(14)	1.80 (11)
Ru(2)–H(12)	1.63 (12)	Ru(4)–H(14)	1.78 (11)
Ru(1)–H(13)	1.58 (11)	Ru(2)–H(23)	1.76 (11)
Ru(3)–H(13)	1.84 (11)	Ru(3)–H(23)	1.52 (12)
average = 1.70 ± 0.12 Å			
(d) Ruthenium–Phosphorus			
Ru(1)–P(1)	2.356 (4)	Ru(2)–P(2)	2.335 (5)
(e) Ruthenium–Carbonyl Carbon			
Ru(1)–C(11)	1.896 (22)	Ru(3)–C(32)	1.902 (18)
Ru(1)–C(12)	1.865 (19)	Ru(3)–C(33)	1.892 (21)
Ru(2)–C(21)	1.856 (19)	Ru(4)–C(41)	1.922 (20)
Ru(2)–C(22)	1.874 (20)	Ru(4)–C(42)	1.850 (19)
Ru(3)–C(31)	1.882 (23)	Ru(4)–C(43)	1.874 (22)
average = 1.881 ± 0.022 Å			
(f) Carbon–Oxygen			
C(11)–O(11)	1.134 (27)	C(32)–O(32)	1.125 (23)
C(12)–O(12)	1.146 (23)	C(33)–O(33)	1.112 (26)
C(21)–O(21)	1.150 (24)	C(41)–O(41)	1.117 (25)
C(22)–O(22)	1.125 (24)	C(42)–O(42)	1.171 (23)
C(31)–O(31)	1.157 (28)	C(43)–O(43)	1.138 (26)
average = 1.138 ± 0.019 Å			
(g) Phosphorus–Carbon and Carbon–Carbon			
P(1)–C(1)	1.816 (18)	P(2)–C(2)	1.835 (16)
P(1)–C(101)	1.814 (16)	P(2)–C(201)	1.804 (16)
P(1)–C(107)	1.839 (16)	P(2)–C(207)	1.829 (17)
C(1)–C(2)	1.570 (23)		
(h) Carbon–Carbon (Phenyl)			
C(101)–C(102)	1.408 (23)	C(104)–C(105)	1.371 (28)
C(102)–C(103)	1.386 (27)	C(105)–C(106)	1.400 (25)
C(103)–C(104)	1.353 (30)	C(106)–C(101)	1.367 (24)
C(107)–C(108)	1.370 (25)	C(110)–C(111)	1.360 (26)
C(108)–C(109)	1.383 (25)	C(111)–C(112)	1.386 (24)
C(109)–C(110)	1.361 (27)	C(112)–C(107)	1.399 (25)
C(201)–C(202)	1.399 (22)	C(204)–C(205)	1.332 (24)
C(202)–C(203)	1.396 (26)	C(205)–C(206)	1.422 (25)
C(203)–C(204)	1.362 (26)	C(206)–C(201)	1.383 (23)
C(207)–C(208)	1.394 (25)	C(210)–C(211)	1.407 (28)
C(208)–C(209)	1.416 (24)	C(211)–C(212)	1.387 (25)
C(209)–C(210)	1.317 (26)	C(212)–C(207)	1.394 (24)
average = 1.381 ± 0.025 Å			

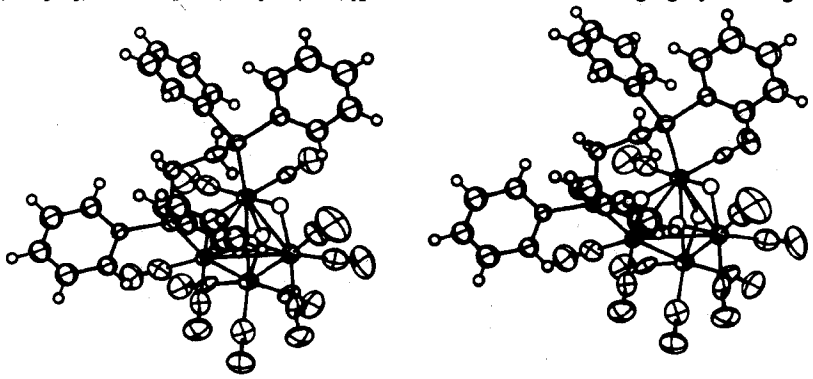

Figure 2. Stereoscopic view of $(\mu\text{-H})_4Ru_4(CO)_{10}(\mu\text{-diphos})$. Ru(1) is at the top, Ru(2) is on the left, Ru(3) is on the right, and Ru(4) is at the bottom of the diagram. This is an ORTEP-II diagram.

Table V. Angles (Deg, with Esd's) within the $(\mu_2\text{-H})_4Ru_4(CO)_{10}(\mu_2\text{-diphos})$ Molecule

atoms	angle	atoms	angle
	(a) Angles within Ru_4 Tetrahedron		
Ru(2)-Ru(1)-Ru(3)	57.66 (4)	Ru(1)-Ru(3)-Ru(2)	61.78 (5)
Ru(2)-Ru(1)-Ru(4)	54.96 (4)	Ru(1)-Ru(3)-Ru(4)	61.57 (5)
Ru(3)-Ru(1)-Ru(4)	55.40 (4)	Ru(2)-Ru(3)-Ru(4)	58.24 (5)
Ru(1)-Ru(2)-Ru(3)	60.56 (5)	Ru(1)-Ru(4)-Ru(2)	63.90 (5)
Ru(1)-Ru(2)-Ru(4)	61.13 (5)	Ru(1)-Ru(4)-Ru(3)	63.04 (5)
Ru(3)-Ru(2)-Ru(4)	58.34 (5)	Ru(2)-Ru(4)-Ru(3)	63.41 (5)
	(b) Angles Involving Hydride Ligands		
Ru(1)-H(12)-Ru(2)	135 (7)	Ru(1)-H(13)-Ru(3)	123 (7)
H(12)-Ru(1)-Ru(2)	22 (4)	H(13)-Ru(1)-Ru(2)	81 (4)
H(12)-Ru(1)-Ru(3)	79 (4)	H(13)-Ru(1)-Ru(3)	31 (4)
H(12)-Ru(1)-Ru(4)	70 (4)	H(13)-Ru(1)-Ru(4)	84 (4)
H(12)-Ru(2)-Ru(1)	22 (4)	H(13)-Ru(3)-Ru(1)	26 (4)
H(12)-Ru(2)-Ru(3)	82 (4)	H(13)-Ru(3)-Ru(2)	81 (4)
H(12)-Ru(2)-Ru(4)	77 (4)	H(13)-Ru(3)-Ru(4)	86 (4)
H(12)-Ru(1)-P(1)	88 (4)	H(13)-Ru(1)-P(1)	83 (4)
H(12)-Ru(1)-C(11)	176 (4)	H(13)-Ru(1)-C(11)	84 (4)
H(12)-Ru(1)-C(12)	85 (4)	H(13)-Ru(1)-C(12)	177 (4)
H(12)-Ru(2)-P(2)	89 (4)	H(13)-Ru(3)-C(31)	91 (4)
H(12)-Ru(2)-C(21)	89 (4)	H(13)-Ru(3)-C(32)	93 (4)
H(12)-Ru(2)-C(22)	178 (4)	H(13)-Ru(3)-C(33)	170 (4)
Ru(1)-H(14)-Ru(4)	112 (6)	Ru(2)-H(23)-Ru(3)	126 (7)
H(14)-Ru(1)-Ru(2)	88 (4)	H(23)-Ru(2)-Ru(1)	65 (4)
H(14)-Ru(1)-Ru(3)	73 (4)	H(23)-Ru(2)-Ru(3)	25 (4)
H(14)-Ru(1)-Ru(4)	34 (4)	H(23)-Ru(2)-Ru(4)	83 (4)
H(14)-Ru(4)-Ru(1)	34 (4)	H(23)-Ru(3)-Ru(1)	68 (4)
H(14)-Ru(4)-Ru(2)	98 (4)	H(23)-Ru(3)-Ru(2)	29 (4)
H(14)-Ru(4)-Ru(3)	80 (4)	H(23)-Ru(3)-Ru(4)	87 (4)
H(14)-Ru(1)-P(1)	170 (4)	H(23)-Ru(2)-P(2)	92 (4)
H(14)-Ru(1)-C(11)	75 (4)	H(23)-Ru(2)-C(21)	169 (4)
H(14)-Ru(1)-C(12)	87 (4)	H(23)-Ru(2)-C(22)	97 (4)
H(14)-Ru(4)-C(41)	78 (4)	H(23)-Ru(3)-C(31)	165 (4)
H(14)-Ru(4)-C(42)	92 (4)	H(23)-Ru(3)-C(32)	90 (4)
H(14)-Ru(4)-C(43)	171 (4)	H(23)-Ru(3)-C(33)	101 (4)
H(12)-Ru(1)-H(13)	98 (6)	H(12)-Ru(2)-H(23)	82 (5)
H(12)-Ru(1)-H(14)	101 (5)	H(13)-Ru(3)-H(23)	76 (6)
H(13)-Ru(1)-H(14)	92 (5)		
	(c) Ru-Ru-CO and Ru-Ru-P Angles		
Ru(2)-Ru(1)-P(1)	99.7 (1)	Ru(1)-Ru(3)-C(31)	97.3 (6)
Ru(3)-Ru(1)-P(1)	105.7 (1)	Ru(2)-Ru(3)-C(31)	142.4 (6)
Ru(4)-Ru(1)-P(1)	153.2 (1)	Ru(4)-Ru(3)-C(31)	84.5 (6)
Ru(2)-Ru(1)-C(11)	157.8 (6)	Ru(1)-Ru(3)-C(32)	116.5 (6)
Ru(3)-Ru(1)-C(11)	102.2 (6)	Ru(2)-Ru(3)-C(32)	118.2 (6)
Ru(4)-Ru(1)-C(11)	107.1 (6)	Ru(4)-Ru(3)-C(32)	176.4 (6)
Ru(2)-Ru(1)-C(12)	102.3 (6)	Ru(1)-Ru(3)-C(33)	144.2 (6)
Ru(3)-Ru(1)-C(12)	151.5 (6)	Ru(2)-Ru(3)-C(33)	91.6 (6)
Ru(4)-Ru(1)-C(12)	97.0 (6)	Ru(4)-Ru(3)-C(33)	84.6 (6)
Ru(1)-Ru(2)-P(2)	104.3 (1)	Ru(1)-Ru(4)-C(41)	110.8 (5)
Ru(3)-Ru(2)-P(2)	117.2 (1)	Ru(2)-Ru(4)-C(41)	166.7 (5)
Ru(4)-Ru(2)-P(2)	165.4 (1)	Ru(3)-Ru(4)-C(41)	103.3 (5)
Ru(1)-Ru(2)-C(21)	104.4 (6)	Ru(1)-Ru(4)-C(42)	98.1 (6)
Ru(3)-Ru(2)-C(21)	146.5 (6)	Ru(2)-Ru(4)-C(42)	96.0 (6)
Ru(4)-Ru(2)-C(21)	88.2 (6)	Ru(3)-Ru(4)-C(42)	156.2 (6)
Ru(1)-Ru(2)-C(22)	155.8 (6)	Ru(1)-Ru(4)-C(43)	148.9 (6)
Ru(3)-Ru(2)-C(22)	96.4 (6)	Ru(2)-Ru(4)-C(43)	86.9 (6)
Ru(4)-Ru(2)-C(22)	101.7 (6)	Ru(3)-Ru(4)-C(43)	95.5 (6)
	(d) CO-Ru-CO and CO-Ru-P Angles		
C(11)-Ru(1)-P(1)	94.9 (6)	C(31)-Ru(3)-C(32)	98.9 (8)
C(12)-Ru(1)-P(1)	97.2 (6)	C(31)-Ru(3)-C(33)	90.2 (9)
C(11)-Ru(1)-C(12)	92.3 (8)	C(32)-Ru(3)-C(33)	96.5 (8)
C(21)-Ru(2)-P(2)	94.9 (6)	C(41)-Ru(4)-C(42)	96.8 (8)
C(22)-Ru(2)-P(2)	92.5 (6)	C(41)-Ru(4)-C(43)	95.3 (8)
C(21)-Ru(2)-C(22)	91.1 (8)	C(42)-Ru(4)-C(43)	95.1 (9)
	(e) Ru-C-O Angles		
Ru(1)-C(11)-O(11)	178.7 (17)	Ru(3)-C(32)-O(32)	174.5 (18)
Ru(1)-C(12)-O(12)	175.9 (18)	Ru(3)-C(33)-O(33)	175.3 (18)
Ru(2)-C(21)-O(21)	178.9 (18)	Ru(4)-C(41)-O(41)	174.3 (16)
Ru(2)-C(22)-O(22)	177.7 (17)	Ru(4)-C(42)-O(42)	178.6 (17)
Ru(3)-C(31)-O(31)	178.8 (18)	Ru(4)-C(43)-O(43)	176.0 (18)
	(f) Ru-P-C and C-P-C Angles		
Ru(1)-P(1)-C(1)	113.0 (5)	C(1)-P(1)-C(101)	100.4 (7)
Ru(1)-P(1)-C(101)	117.2 (5)	C(1)-P(1)-C(107)	105.4 (7)
Ru(1)-P(1)-C(107)	115.0 (6)	C(101)-P(1)-C(107)	104.2 (7)

Table V (*Continued*)

atoms	angle	atoms	angle
Ru(2)-P(2)-C(2)	111.9 (5)	C(2)-P(2)-C(201)	102.2 (7)
Ru(2)-P(2)-C(201)	115.3 (5)	C(2)-P(2)-C(207)	102.7 (7)
Ru(2)-P(2)-C(207)	120.7 (6)	C(201)-P(2)-C(207)	101.7 (7)
	(g) P-C-C Angles		
P(1)-C(1)-C(2)	115.6 (11)	P(2)-C(2)-C(1)	111.2 (11)
P(1)-C(101)-C(102)	118.9 (13)	P(2)-C(201)-C(202)	123.5 (12)
P(1)-C(101)-C(106)	123.2 (13)	P(2)-C(201)-C(206)	119.4 (12)
P(1)-C(107)-C(108)	124.8 (13)	P(2)-C(207)-C(208)	120.8 (12)
P(1)-C(107)-C(112)	116.6 (12)	P(2)-C(207)-C(212)	121.4 (13)
	(h) Phenyl C-C-C Angles		
C(106)-C(101)-C(102)	117.8 (16)	C(206)-C(201)-C(202)	116.7 (14)
C(101)-C(102)-C(103)	119.4 (17)	C(201)-C(202)-C(203)	120.7 (15)
C(102)-C(103)-C(104)	122.4 (19)	C(202)-C(203)-C(204)	121.0 (17)
C(103)-C(104)-C(105)	118.7 (19)	C(203)-C(204)-C(205)	119.8 (17)
C(104)-C(105)-C(106)	120.2 (18)	C(204)-C(205)-C(206)	120.5 (16)
C(105)-C(106)-C(101)	121.4 (17)	C(205)-C(206)-C(201)	121.0 (15)
C(112)-C(107)-C(108)	118.6 (15)	C(212)-C(207)-C(208)	117.6 (16)
C(107)-C(108)-C(109)	119.1 (16)	C(207)-C(208)-C(209)	119.5 (16)
C(108)-C(109)-C(110)	122.2 (17)	C(208)-C(209)-C(210)	122.2 (18)
C(109)-C(110)-C(111)	119.5 (17)	C(209)-C(210)-C(211)	119.8 (18)
C(110)-C(111)-C(112)	119.6 (16)	C(210)-C(211)-C(212)	119.1 (17)
C(111)-C(112)-C(107)	120.9 (16)	C(211)-C(212)-C(207)	121.7 (17)

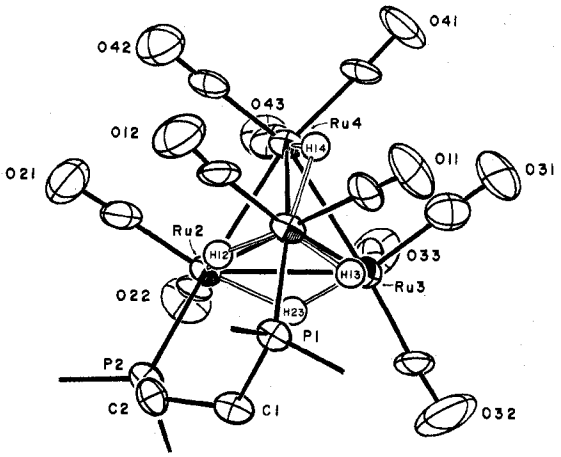

Figure 3. $(\mu\text{-H})_4Ru_4(CO)_{10}(\mu\text{-diphos})$ molecule, with phenyl groups and methylene hydrogens [on C(1) and C(2)] omitted. The molecule is projected on to the Ru(2)–Ru(3)–Ru(4) plane; Ru(1) is unlabeled and occupies the apex of the tetrahedron in the center of the figure. Carbon atoms of the carbonyl groups are numbered identically with their attached oxygen atoms. This is an ORTEP-II diagram.

of possible orientations relative to the bridged metal–metal vector. For any regular $(\mu_2\text{-H})_nM_4L_{12}$ species ($1 < n < 8$; L = normal donor ligand), there are two probable idealized locations of a hydride ligand about a given metal vector as shown in V and VI. In V the bridging hydride ligand about

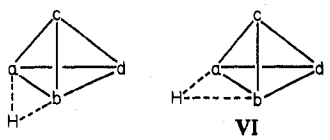

V VI

a–b is approximately coplanar with abc or approximately perpendicular to abd; in VI, the bridging hydride ligand is approximately coplanar with abd or approximately perpendicular to abc.

The locations of the bridging hydride ligands in the present $(\mu\text{-H})_4Ru_4(CO)_{10}(\mu\text{-diphos})$ molecule are defined as follows. [Here the prefix "dev" indicates the deviation of an atom from a defined plane.]

Atom H(12) bridges Ru(1) and Ru(2) and lies +0.19 (11) Å from the Ru(1)–Ru(2)–Ru(3) plane, being displaced in a direction away from Ru(4) [dev(Ru(4)) = −2.254 (1) Å]; deviations from the Ru(1)–Ru(2)–Ru(4) plane are dev(H(12)) = −0.48 (10) Å and dev(Ru(3)) = +2.357 (1) Å.

H(13) spans the Ru(1)–Ru(3) vector and is closer to planarity with the Ru(1)–Ru(3)–Ru(4) plane [dev(H(13)) = +0.30 (13) Å, dev(Ru(2)) = −2.373 (2) Å] than with the Ru(1)–Ru(2)–Ru(3) plane [dev(H(13)) = +0.57 (11) Å, dev(Ru(4)) = −2.254 (1) Å].

H(14) spans the Ru(1)–Ru(4) linkage and is coplanar, within experimental error, with the Ru(1)–Ru(2)–Ru(4) face of the Ru_4 tetrahedron [dev(H(14)) = −0.10 (10) Å, dev(Ru(3)) = +2.357 (1) Å]; deviations with respect to the Ru(1)–Ru(3)–Ru(4) face are dev(H(14)) = +0.92 (12) Å and dev(Ru(2)) = −2.373 (2) Å.

Finally, H(23) lies +0.17 (11) Å from the Ru(2)–Ru(3)–Ru(4) plane [dev(Ru(1)) = +2.529 (1) Å] and +0.74 (11) Å from the Ru(1)–Ru(2)–Ru(3) plane [dev(Ru(4)) = −2.254 (1) Å].

The ten carbonyl ligands are in terminal positions, with individual ruthenium–carbonyl distances ranging from 1.850 (19) to 1.922 (20) Å and averaging 1.881 ± 0.022 Å. Carbon–oxygen bond lengths range from 1.112 (26) to 1.171 (23) Å, the mean of the ten values being 1.138 ± 0.019 Å. The diphos ligand is in an unusual bridging location and is linked to the cluster by the ruthenium–phosphorus bonds Ru(1)–P(1) = 2.356 (4) Å and Ru(2)–P(2) = 2.335 (5) Å. The geometry of the six membered Ru(1)–P(1)–C(1)–C(2)–P(2)–Ru(2) ring is clearly shown in Figure 2. All bond lengths and bond angles have the expected values; the planarity of the phenyl rings is shown in Table VI.

Solution Structure and Dynamics of $(\mu\text{-H})_4Ru_4(CO)_{10}(\mu\text{-diphos})$

The diphos ligand configurations in isomers I and II of $(\mu\text{-H})_4Ru_4(CO)_{10}$(diphos) are nicely distinguished on the basis of ^{31}P NMR data. It has been noted several times that a phosphorus atom involved in a five-membered chelate ring experiences anomalously large nuclear deshielding upon coordination.[14] Garrou has expressed this phenomenon in terms of a ring-effect parameter Δ_R.[15] The sign and magnitude of

(12) Churchill, M. R.; Hollander, F. J. *Inorg. Chem.* **1979**, *18*, 161.
(13) Churchill, M. R.; Hollander, F. J. *Inorg. Chem.* **1979**, *18*, 843.
(14) Grim, S. O.; Briggs, W. L.; Barth, R. C.; Tolman, C. A.; Jesson, J. P. *Inorg. Chem.* **1974**, *13*, 1095.

Table VI. Least-Squares Planes[a,b] and Deviations of Atoms Therefrom[c]

atom	dev, Å	atom	dev, Å
Plane I: $0.8030X - 0.4355Y - 0.4068Z = 4.5756$			
C(101)*	0.0048	C(105)*	−0.0103
C(102)*	−0.0107	C(106)*	0.0027
C(103)*	0.0063	P(1)	0.0733
C(104)*	0.0061	Ru(1)	−0.3868
Plane II: $-0.2814X + 0.3858Y - 0.8786Z = 4.4365$			
C(107)*	−0.0204	C(111)*	0.0050
C(108)*	0.0240	C(112)*	0.0090
C(109)*	−0.0093	P(1)	−0.0565
C(110)*	−0.0056	Ru(1)	−1.7416
Plane III: $0.5926X + 0.3499Y - 0.7255Z = 9.1429$			
C(201)*	0.0174	C(205)*	0.0144
C(202)*	−0.0132	C(206)*	−0.0200
C(203)*	0.0048	P(2)	−0.0859
C(204)*	−0.0038	Ru(2)	−2.1800
Plane IV: $-0.6056X + 0.6337Y - 0.4814Z = 2.2165$			
C(207)*	0.0069	C(211)*	−0.0027
C(208)*	0.0025	C(212)*	−0.0090
C(209)*	−0.0161	P(2)	0.1418
C(210)*	0.0157	Ru(2)	−0.1730

[a] Equations to planes are expressed in orthonormal coordinates (X, Y, Z) which are related to the fractional coordinates (x, y, z) via the transformation:

$$\begin{pmatrix} X \\ Y \\ Z \end{pmatrix} = \begin{pmatrix} a & 0 & c\cos\beta \\ 0 & b & 0 \\ 0 & 0 & c\sin\beta \end{pmatrix} \begin{pmatrix} x \\ y \\ z \end{pmatrix}$$

[b] Only atoms marked with an asterisk were included in calculation of the plane. [c] Important interplanar angles are plane I − plane II = 92.09° and plane III − plane IV = 77.75°.

Table VII. ^{31}P NMR Data for the Isomers of $H_4Ru_4(CO)_{10}(Ph_2PCH_2CH_2PPh_2)$ and for $H_4Ru_4(CO)_{10}(PPh_2Me)_2$

	T, °C	δ_{coord}[a]	δ_{free}[a]	Δ[b]	Δ_R[c]
isomer I	−50[d]	70.2 (d)[e]	−12.5[f]	+82.7	+35.4
		63.0 (d)[e]		+75.5	+28.2
isomer II	−101[g]	41.8 (s)	−12.5[f]	+54.3	+7.0
		30.4 (s)		+42.9	−4.4
$H_4Ru_4(CO)_{10}(PPh_2Me)_2$	−50[d]	19.6 (s)	−27.7[h]	+47.3	

[a] In parts per million downfield of 85% H_3PO_4. [b] $\Delta = \delta_{coord} - \delta_{free}$. [c] $\Delta_R = \Delta[H_4Ru_4(CO)_{10}(diphos)] - \Delta[H_4Ru_4(CO)_{10}(PPh_2Me)_2]$; see ref 15. [d] In $CDCl_3$. [e] $J_{PP} = 17$ Hz. [f] Reference 14. [g] In $CD_2Cl_2/CHFCl_2$. [h] Reference 16.

Δ_R depend on the size of the ring involving the phosphorus center. It is large and positive for five-membered rings, smaller and negative for four-membered rings, and close to zero for six-membered rings. As can be seen from the data in Table VII, the ^{31}P chemical shifts for isomer I are significantly downfield of those for isomer II. The ring-effect parameters can be calculated by using $(\mu\text{-H})_4Ru_4(CO)_{10}(PPhMe_2)_2$ as a reference. These Δ_R values are consistent with the presence of a five-membered Ru–P–C–C–P ring in isomer I and a six-membered Ru–P–C–C–P–Ru ring in isomer II as observed in the respective crystal structures.

The ^{1}H NMR resonances of the hydride ligands in $(\mu\text{-H})_4Ru_4(CO)_{10}(\mu\text{-diphos})$ as they appear at several temperatures are displayed in Figure 4. The single, sharp triplet (J = 3 Hz) at τ 27.3 that is present in the room-temperature spectrum first broadens and then separates into new patterns as the sample temperature is lowered. At −92 °C there are four signals of equal intensity. Two of these are moderately sharp triplets at τ 28.9 (A, J = 17 Hz) and 25.9 (B, J = 16 Hz), whereas two appear as broad humps near τ 26.8 and 27.3 (C and D). At −131 °C only very broad, featureless peaks are discernible at the approximate positions τ 25.5, 25.9, 28.2, and 28.9 (calcd mean τ 27.1). The compound crystallizes extensively from solution at lower temperatures, which prevented our achieving a limiting spectrum. Nevertheless, if we assume that the solid-state configuration is maintained in solution, the spectral changes are readily interpreted in terms of three dynamic processes.

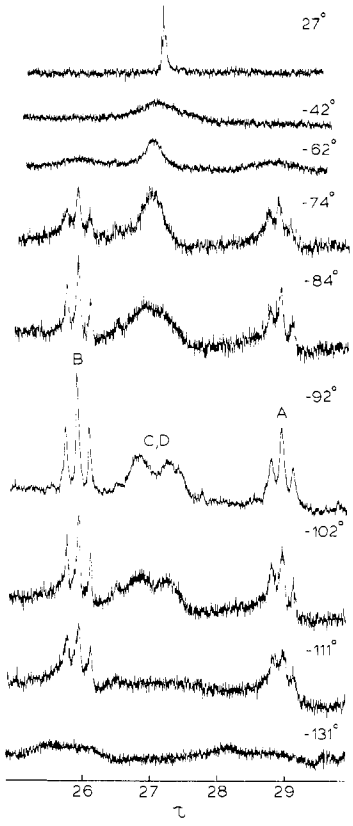

Figure 4. Variable-temperature ^{1}H NMR spectra of $(\mu\text{-H})_4Ru_4(CO)_{10}(\mu\text{-diphos})$ in the hydride-ligand region.

The lowest energy process affects the hydride ligand signals from below −131 to −92 °C. The broad humps at τ 25.9 and 28.9 sharpen into the triplets A and B, whereas the humps near τ 25.5 and 28.2 seem first to disappear and then to reappear at τ 26.8 and 27.3 (C and D). The triplet patterns suggest equivalent phosphorus centers, but if this were strictly true for two of the hydrides, it would have to be true for the other two as well. Therefore, the triplets are only apparent, resulting from nearly equal values of $|J(P\text{–}H)|$. The situation can arise in the following way. Refer to Figure 3, and consider only the $(\mu\text{-H})_4Ru_4P_2$ portion of the molecule. Movement of H(14) from the Ru(1)–Ru(4) edge to the Ru(2)–Ru(4) edge would produce a mirror-image configuration in which H(14) is trans to P(2) and the relative positions of H(13) and H(23) are interchanged. If exchange of H(14) between the two edges were rapid, the NMR signals of the hydride ligands (considering only P–H couplings) would be triplets for H(14) and H(12) and the A portion of an AA′XX′ pattern for H(13) and H(23). However, *the backbone of the diphos ligand is asymmetric.* If its conformational averaging is slower than the migration of H(14), the two configurations related by the migration are not enantiomers. The appearance of the averaged signals for the hydride ligands will depend on the degree of similarity in the exchange-related environments.

Refer now to Figure 5 where our proposal for the lowest energy process is diagrammed. For convenience the signals observed in the −92 °C spectrum have been assigned to the

(15) Garrou, P. E. *Inorg. Chem.* **1975**, *14*, 1435.
(16) Mann, B. E.; Masters, C.; Shaw, B. L. *J. Chem. Soc. A* **1971**, 1104.

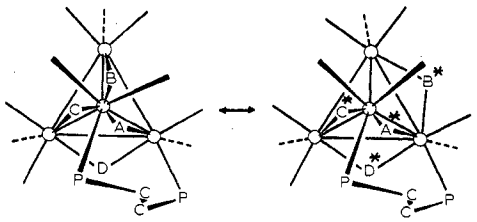

Figure 5. Proposed mechanism for the lowest energy dynamic process in $(\mu\text{-H})_4Ru_4(CO)_{10}(\mu\text{-diphos})$.

hydride ligand positions as follows: H_A = H(12), H_B = H(14), H_C = H(13), H_D = H(23). Reversing the assignments in the pairs A,B or C,D does not affect the argument. Migration of H_B to the position of H_B* changes H_A to H_A*, H_C to H_D*, and H_D to H_C*. It appears that the diastereomeric environments are sufficiently similar for H_B/H_B* and for H_A/H_A* that only one signal, a triplet, results in each case. On the other hand the diphos backbone configuration, or the concomitant phenyl ring orientations, appears to influence the H_C/H_{C*} and H_D/H_{D*} environments to the extent that the averaged signals H_C/H_D* and H_D/H_C* are distinct. The residual line widths of these signals in the −92 °C spectrum presumably result from unresolved P–H as well as H–H couplings.

The second process affects the spectra over the temperature range from −92 to −74 °C. The separate broad humps (C and D) at τ 26.8 and 27.3 coalesce into one broad resonance, whereas the triplet signals (A and B) are not appreciably affected. We interpret this as due to conformational changes in the diphos ligand that suffice to generate an effective mirror plane and completely equilibrate H_C and H_D. With the values $\Delta\nu$ = 50 Hz and T_c = −84 °C (189 K), the free energy of activation for this process can be estimated as $\Delta G_c^{\ddagger}$ = 9.1 kcal/mol, which compares with $\Delta G_c^{\ddagger}$ = 7.2 kcal/mol ($\Delta\nu$ = 270 Hz, T_c = 162 K) for the first process.[17]

The final dynamic process, which totally equilibrates the hydride ligands, is seen above −74 °C and occurs rapidly above −40 °C. In order for the averaged triplet signal to display such a small splitting (3 Hz), the much larger splittings (16 and 17 Hz) seen in the triplet signals at −92 °C must be opposite in sign. This requirement is easily rationalized in terms of the solid-state structure (see Figure 3) together with coupling constant data for isomer I. Thus, H(14) is approximately trans to P(1) and three bonds removed from P(2). In isomer I, similar three-bond couplings were too small to resolve, whereas $J(P\text{–}H)_{trans}$ was large, 29–31 Hz. Therefore, in the case of isomer II, when H(14) oscillates rapidly between the edges trans to P(2) and P(1), the average coupling constant will be essentially equal to $J(P\text{–}H)_{trans}/2$, or about 15 Hz. On the other hand, H(13) is approximately cis to P(1), H(23) is cis to P(2), and H(12) is cis to both phosphorus centers. In isomer I the values of $J(P\text{–}H)_{cis}$ ranged from 9 to 18 Hz, and in one clear case the sign was opposite to that of $J(P\text{–}H)_{trans}$. Thus, the triplet splittings seen in the −92 °C spectrum are consistent with both $J(P\text{–}H)_{cis}$ and $J(P\text{–}H)_{trans}/2$. Furthermore, an average taken over all four sites will reflect the three medium-sized couplings of one sign together with the larger one of opposite sign. Taking approximate values as an example, $|J_{av}| = {}^1/_2|J(P_1\text{–}H)_{av} + J(P_2\text{–}H)_{av}| \simeq {}^1/_2|(-30 + 14 + 14 + 0)/4 + (0 + 14 + 0 + 14)/4| \simeq 3$ Hz.

In our previous study of hydride mobility in isomer I,[2] analysis of the exchange-broadened line shapes supported a mechanism involving intermediate configurations with the hydride ligands in terminal positions. In the present case either terminal or face-bridged intermediate configurations can be drawn for the lowest energy process involving H_B (Figure 5). Unfortunately, no distinction can be made on the basis of the experimental spectra. For the highest energy process a mechanism involving terminal intermediates would not equilibrate H_B with the other three hydride ligands if only the C_s hydride configuration (see III) is accessible. However, complete scrambling via terminal intermediates can occur, if traversal of slightly higher energy D_{2d} configurations (see IV) is possible. Alternatively, face-bridged intermediates would suffice for complete scrambling without involvement of D_{2d} configurations. A recent theoretical study of hydride-ligand configurations in $(\mu\text{-H})_4M_4$ molecules indicated rather small energy differences between D_{2d} edge-bridged [as in $(\mu\text{-H})_4Ru_4(CO)_{12}$] and T_d face-bridged [as in $(\mu_3\text{-H})_4Co_4(\eta^5\text{-}C_5H_5)_4$] structures.[18] The edge-bridged configuration of C_s symmetry (III) was not examined directly in the calculations. Nevertheless, the fact that $(\mu\text{-H})_4Ru_4(CO)_{11}[P(OMe)_3]$ and $(\mu\text{-H})_4Ru_4(CO)_{10}(PPh_3)_2$ adopt configuration IV whereas the two isomers of $(\mu\text{-H})_4Ru_4(CO)_{10}$(diphos) adopt configuration III suggests that these two arrangements also differ little in energy. However, since it is uncertain at present what factors determine the ground-state hydride-ligand configurations in derivatives of $(\mu\text{-H})_4Ru_4(CO)_{12}$, it is also not clear what higher energy configurations are most accessible for hydride-scrambling pathways. These questions remain for further study.

Acknowledgment. This work was generously supported by the National Science Foundation through Grant No. CHE77-04981 to M.R.C. and No. CHE76-14460 to J.R.S. Field-desorption mass spectra were obtained in part with support from the National Institute of General Medical Sciences (Grant No. GM 27029).

Registry No. $(\mu\text{-H})_4Ru_4(CO)_{10}(\mu\text{-diphos})$, 73037-73-7; $(\mu\text{-H})_4Ru_4(CO)_{12}$, 34438-91-0; $(\mu\text{-H})_4Ru_4(CO)_{10}$(diphos), 66322-95-0; $(\mu\text{-H})_4Ru_4(CO)_{10}(PPh_2Me)_2$, 73037-72-6.

Supplementary Material Available: Listing of structure factor amplitudes (13 pages). Ordering information is given on any current masthead page.

(17) The equations used for the calculations are $k_c = 2^{1/2}(\pi/2)\Delta\nu$ and $\Delta G_c^{\ddagger} = 2.303RT_c[\log(k_B/h) - \log(k_c/T_c)]/1000$.

(18) Hoffmann, R.; Schilling, B. E. R.; Bau, R.; Kaesz, H. D.; Mingos, D. M. P. *J. Am. Chem. Soc.* **1978**, *100*, 6088.